BMC Public Health

RESEARCH

Open Access

Joint spatiotemporal modelling of tuberculosis and human immunodeficiency virus in Ethiopia using a Bayesian hierarchical approach

Legesse Kassa Debusho[1*†] and Leta Lencha Gemechu[1†]

Abstract

Background The aim of this paper was to evaluate the distribution of HIV and TB in Ethiopia during four years (2015-2018) at the district level, considering both spatial and temporal patterns.

Methods Consolidated data on the count of TB case notifications and the number of patients with HIV for four years, 2015-2018, were provided by the Ethiopian Federal Ministry of Health. The data was analyzed using the Bayesian hierarchical approach, employing joint spatiotemporal modelling. The integrated nested Laplace approximation available in the R-INLA package was used to fit six models, each with different priors, for the precision parameters of the random effects variances. The best-fitting model with the best predictive capacity was selected using the Deviance Information Criterion and the negative sum of cross-validatory predictive log-likelihood.

Results According to the findings of the selected model, about 53% of the variability in TB and HIV incidences in the study period was explained by the shared temporal component, disease-specific spatial effect of HIV, and space-time interaction effect. The shared temporal trend and disease-specific temporal trend of HIV risk showed a slight upward trend between 2015 and 2017, followed by a slight decrease in 2018. However, the disease-specific temporal trend of TB risk had almost constant trend with minimal variation over the study period. The distribution of the shared relative risks was similar to the distribution of disease-specific TB relative risk, whereas that of HIV had more districts as high-risk areas.

Conclusions The study showed the spatial similarity in the distribution of HIV and TB case notifications in specific districts within various provinces. Moreover, the shared relative risks exhibit a temporal pattern and spatial distribution that closely resemble those of the relative risks specific to HIV illness. The existence of districts with shared relative risks implies the need for collaborative surveillance of HIV and TB, as well as integrated interventions to control the two diseases jointly.

Keywords Bayesian hierarchical, HIV, Poisson regression, Relative risk, Joint spatiotemporal modelling, Tuberculosis

†Legesse Kassa Debusho and Leta Lencha Gemechu contributed equally to this work.

*Correspondence:
Legesse Kassa Debusho
debuslk@unisa.ac.za
Full list of author information is available at the end of the article

Background

Human immunodeficiency virus (HIV) and tuberculosis (TB) are epidemiologically associated [1]. The observed co-dynamics indicate a direct relationship between the two diseases, both *at the population level* [2] and *within the host* [3]. Despite being a disease that may be prevented and treated, TB remains the primary cause of mortality for individuals living with HIV [4]. The HIV pandemic has significantly influenced the rates of TB incidence as well [5]. It is predicted that people living with HIV (PLHIV) have a twentyfold increased likelihood of getting active TB in comparison to those who do not have HIV [6].

According to a study conducted in Ethiopia, there is a significant relationship between the occurrence of TB and the level of HIV infection [7]. Following the WHO recommendation, the Ethiopian government has implemented various strategies, for example expansion of the integrated service for TB and HIV to the health care facilities, to manage TB and HIV [8]. Despite the implemented interventions, Ethiopia continues to be one of the 30 countries identified in the 2021 WHO Global TB Report as having a high prevalence of TB and HIV from 2015 to 2020 [9].

TB and HIV are generally related diseases; therefore, their geographical patterns should hypothetically show standard features. Association between these patterns may serve as a second source of dependence to improve risk estimates of these diseases [10]. The spatiotemporal analysis enables us to investigate the continuation of a disease pattern throughout time simultaneously and can also help in identifying atypical disease patterns. The continuation could point to some potential factors that could impact prevalence of the disease, such as environmental factors, which assist in the interpretation of spatial patterns. Within the same spatiotemporal analysis, it is also possible to include space-time interaction terms to investigate the presence of localized clusters that may link to some environmental factors, strengthening the statistical inferences [11].

When conducting joint disease mapping research, each spatial unit is associated with at least two outcomes, such as the incidence of two diseases instead of only one. Since joint models use other additional response variables as an additional information source, this could improve risk estimates. Suppose there is a dependence between the two diseases. In that case, their dependence leads to sharing information between the two outcomes in the modeling process, which could improve risk estimates [10]. Various researchers in the disease mapping field have focused on applying the Bayesian joint spatial and spatiotemporal modeling of multiple diseases, see, e.g., [11–17]. Multiple studies conducted in Ethiopia have examined, separately at various levels, the spatial clustering and temporal trend of HIV and TB [18–23]. However, study to assess the joint spatiotemporal pattern of HIV and TB incidences and to identify locations with high-risk somewhat lacking in the country. This paper aimed to assess the distribution of HIV and TB relative risk in Ethiopia during four years (2015–2018) at the district level, considering both spatial and temporal patterns. The modeling framework in the statistical analysis was formulated via the Bayesian hierarchical modeling approach. The Bayesian hierarchical joint spatiotemporal modeling (BHJSTM) of two related diseases helps to strengthen inference as the modeling allows the borrowing of information between diseases. The BHJSTM utilises the combined power of data from several districts and years to generate smoothed estimates at the district level for each year. It also enables the investigation of geographical and temporal heterogeneity. In addition, it helps quantify the anticipated heterogeneity linked to potential risk factors and extract distinct patterns associated with each disease under investigation from the residual variations [11].

Methods

Study area

Ethiopia is situated in Africa's northeastern region. The country's administrative divisions, before 2021, were two city administrations, Addis Ababa and Dire Dawa; and nine regional states, including Tigray, Afar, Amhara, Oromia, Somali, Benishangul-Gumuz, Southern Nations, Nationalities, and Peoples' (SNNP), Gambella, and Harari. Each regional state has additional divisions known as zones, which are further divided into districts (also known as "woreda") and districts into Kebeles. Figure 1[1] shows the spatial plot of Ethiopia's zones and regions. The regional states are responsible for providing public services because of the transfer of authority to regional governments. The districts oversee service planning and execution, while the regional health bureaus oversee public health administration.

Source of study data

The dataset utilised in this study included the count of individuals diagnosed with HIV who registered at HIV health care facilities and the number of district-level TB case notifications of individuals who registered in Directly Observed Therapy, Short Course (DOTS). The

[1] This map was taken from the web site https://en.m.wikipedia.org/wiki/File:Map_of_zones_of_Ethiopia.svg. Note that the new regions South West Ethiopia Peoples' Region, South Ethiopia Regional State, Central Ethiopia Regional State, and Sidama region are part of the Southern Nations, Nationalities, and Peoples'(SNNP).

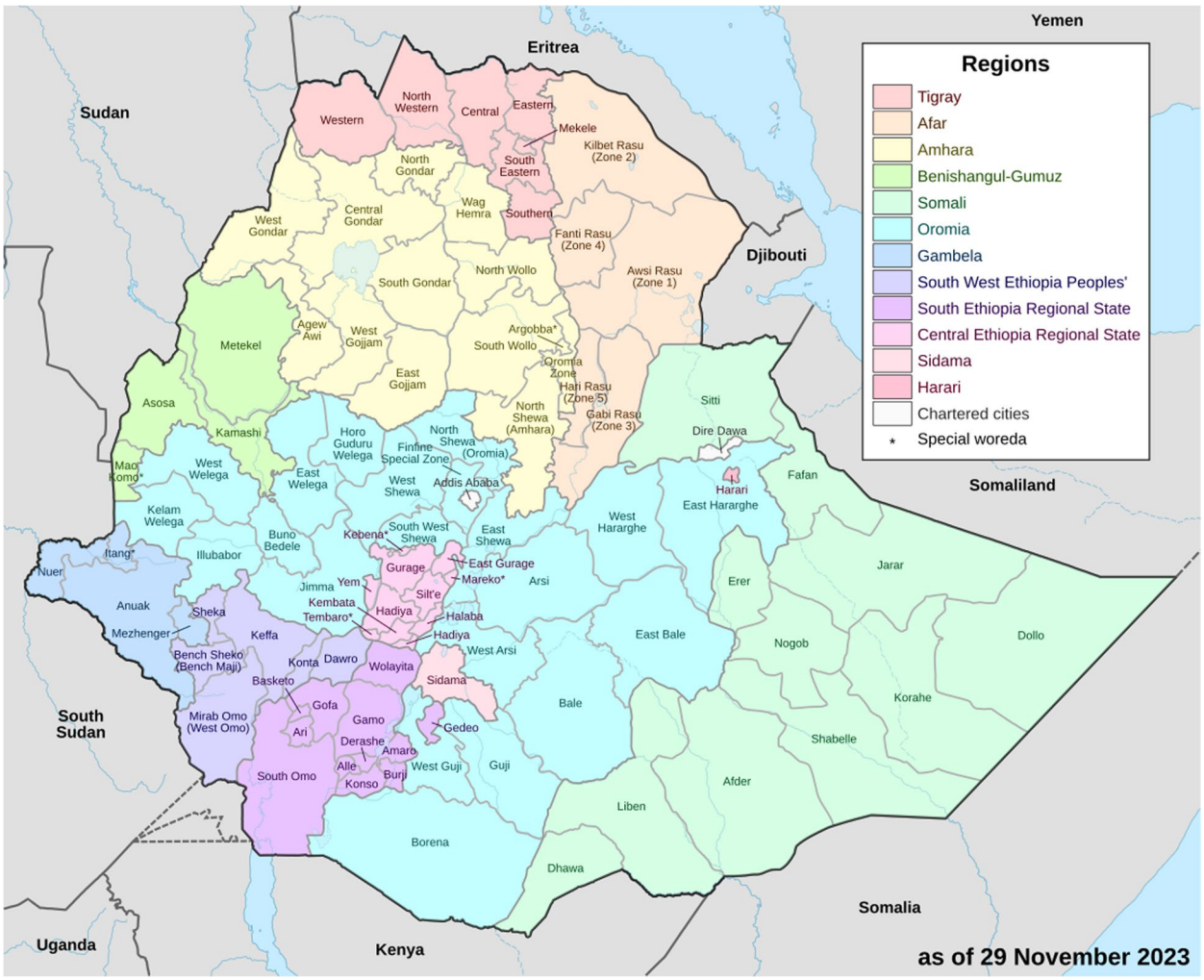

Fig. 1 Geographical maps showing Ethiopia's various zones and provinces. The abbreviations E, N, S, W, C, and Sp respectively represent east, north, south, west, northwest, and special

District Health Office reports the dataset quarterly or yearly to the Federal Ministry of Health (FMoH) via the Health Management Information System (HMIS) [24, 25]. The study dataset, therefore, were obtained from FMoH. In addition to this dataset, the FMoH also provided shape files for district mapping, which were created by Ethiopia's Central Statistics Agency (CSA).

Bayesian hierarchical joint spatiotemporal modelling for TB and HIV

In this paper, we assessed the spatiotemporal variation of HIV and TB risks by jointly analysing data of the two diseases obtained from HMIS. We applied a Bayesian hierarchical model approach. The Bayesian hierarchical model estimates the posterior distributions of the parameters in the model by applying a hierarchical order using the Bayes method. In order to estimate the posterior distribution, the observed data via the likelihood function is joined with the prior distributions of model parameters by the Bayes theorem. The Bayesian hierarchical joint spatiotemporal modeling allows the splitting of risks of diseases into two spatiotemporal components: shared and disease-specific.

Let y_{dit} be the d disease cases notifications for district i in year t, i, $i = 1, \ldots, M$, $t = 1, \ldots, T$, and $d = 1$ and $d = 2$ represent HIV and TB diseases, respectively. We assume that each observed case notification y_{dit} follows the Poisson distribution with mean μ_{dit}, and the mean is calculated as $\mu_{dit} = E_{dit} \times \theta_{dit}$, where θ_{dit} is the unknown relative risk of d disease and E_{dit} is the expected number of d disease case notifications. Therefore, $y_{dit}|E_{dit}, \theta_{dit} \sim Poisson(\mu_{dit})$. The expected case

notifications E_{dit} represents the number of case notifications for d disease that one would anticipate if district i's population behaved like the general population.

Let N_d be the number of general population, then N_d defined as the average of the pooled district population estimates for the study period, i.e., $N_d = \sum_{i=1}^{M}\sum_{t=1}^{T} n_{dit}/T$, where n_{dit} is the estimated population of district i at time t is considered as the population at risk of d disease, with $T = 4$ for the current study. The crude rate for d disease was then calculated as $\hat{\theta}_{dit} = m_{dit}/n_{dit}$, where m_{dit} is the number of cases notifications of disease d in district i in year t. The expected cases notification E_{dit} for d disease was estimated for district i in year t as $E_{dit} = N_d \times \hat{\theta}_{dit}$ [26]. Then a joint spatiotemporal Poisson regression model for the relative risks θ_{dit} for the two diseases are defined in a logarithmic scale as

$$\begin{cases} \eta_{1it} = log(\mu_{1it}) = \alpha_1 + \omega_i\delta + \phi_t\kappa + \nu_{1i} + \gamma_{1t} + \psi_{it}, \\ \eta_{2it} = log(\mu_{2it}) = \alpha_2 + \frac{\omega_i}{\delta} + \frac{\phi_t}{\kappa} + \nu_{2i} + \gamma_{2t} + \psi_{it} \end{cases} \quad (1)$$

where α_d is disease-specific intercepts, ω_i and ϕ_t are shared spatial random effect, shared temporal random effect, ν_{di} and γ_{dt} are disease-specific spatial and disease-specific temporal random effects, and ψ_{it} is a common random interaction effect between space and time, δ is a spatial scaling parameter or weight and κ is a temporal scaling parameter or weight. The effects of the shared spatial random effect ω_i and temporal random effect, ϕ_t, on the relative risks of HIV and TB are modulated via weights δ and κ, respectively [11, 27]. This weighting allows each disease to have its own risk gradients on ω_i and ϕ_t. Unlike [16], the model in Expression (1) includes a random interaction effect between space and time. The disease-specific spatial and disease-specific temporal effects, ν_{di} and γ_{dt}, in the above model allow for departures from any ω_i and ϕ_t, that is, the diseases HIV and TB may have different spatial pattern or temporal trend. Whereas the common space-time interaction random effect, ψ_{it} provides additional flexibility towards identifying varying patterns.

Computation and models comparison

Let $\boldsymbol{\nu}_d = (\nu_{d1}, \ldots, \nu_{dN})$ and $\boldsymbol{\gamma}_d = (\gamma_{d1}, \ldots, \gamma_{dT})$ are vectors of disease-specific spatial random effects and disease-specific temporal random effects, respectively, and $\boldsymbol{\omega}_d = (\omega_{d1}, \ldots, \omega_{dN})$ and $\boldsymbol{\phi}_d = (\phi_{d1}, \ldots, \phi_{dT})$ are vectors of shared spatial random effects and shared temporal random effects.

The classical Bayesian inference approach uses the Markov Chain Monte Carlo (MCMC) technique [28]. Since the MCMC technique requires a significant amount of time for analysis, the models in Expression (1) were fitted numerically by applying the integrated nested Laplace approximation (INLA) method [29]. In order to apply a Bayesian method, the stochastic components of the model need prior distributions. We assumed spatially correlated prior distributions for the shared random effects and disease-specific random effects [11]. Specifically, we modeled them using an intrinsic Conditional Autoregressive (iCAR) structure. Using an element of vector $\boldsymbol{\nu}_d$, ν_{di}, iCAR defined as

$$\nu_{di}|\boldsymbol{\nu}_{d(-i)}, \tau_{\nu_d}, \mathbf{W} \sim Normal\left(\frac{\sum_{j\in\triangle_i}\nu_{dj}}{\mathcal{N}_i}, \frac{\tau_{\nu_d}}{\mathcal{N}_i}\right),$$

where vector $\boldsymbol{\nu}_{d(-1)}$ represents the set of disease-specific random effects excluding ν_{di} for disease d, τ_{ν_d} is an unknown precision parameter, $\triangle_i$ represents the neighbours of the ith district according to the definition of a symmetric binary weights matrix $\mathbf{W}$; $\mathcal{N}_i$ is the number of neighbouring districts of the ith district and its value also is equal to the sum of the ith row of the $\mathbf{W}$ matrix [30].

The iCAR model for elements of $\boldsymbol{\omega}_d$ can easily be written following the above definition. In matrix form these can also be defined as

$$\boldsymbol{\nu}_d \sim iCAR(\mathbf{W}, \tau_{\nu_d}\mathbf{I}) \quad \text{and} \quad \boldsymbol{\omega}_d \sim iCAR(\mathbf{W}, \tau_{\omega_d}\mathbf{I}),\ d = 1, 2.$$

Note that for shared and disease-specific temporal effects, we have used a temporal adjacency structure $\mathbf{Q}$ [31]. Assume there is yearly fluctuations in elements of $\boldsymbol{\gamma}_d$ and $\boldsymbol{\phi}_d$. Then to reflect this in the priors, in this paper, we have employed a first order random walk (RW1) to model $\boldsymbol{\gamma}_d$ and $\boldsymbol{\phi}_d$. This modelling also involves the use of a weighted matrix $\mathbf{Q}$ to define the temporal neighborhood. Or, using $\gamma_{dt} \in \boldsymbol{\gamma}_d$, RW1 is defined as

$$\gamma_{dt}|\boldsymbol{\gamma}_{d(-t)} \sim \begin{cases} Normal(\gamma_{d(t-1)}, \sigma^2_{\gamma_d}) & \text{for } t = 1, \\ Normal\left(\frac{\gamma_{d(t-1)}+\gamma_{d(t+1)}}{2}, \frac{\sigma^2_{\gamma_d}}{2}\right) & \text{for } t = 2, \ldots, T-1, \\ Normal(\gamma_{d(t-1)}, \sigma^2_{\gamma_d}) & \text{for } t = T; \end{cases}$$

where $\boldsymbol{\gamma}_{d(-t)}$ denotes all elements of $\boldsymbol{\gamma}_d$ except the γ_{dt}. We used improper flat prior for disease-specific intercepts α_d, $d = 1, 2$. As in [16], $\delta \sim log - Normal(0, 1/5.9)$ and $\kappa \sim log - Normal(0, 1/5.9)$. The space-time random interaction effect, ψ_{it} was specified by a Gaussian exchangeable prior $\psi_{it} \sim Normal(0, 1/\tau^2_\psi)$ where τ_ψ is precision parameter of ψ_{it}.

We have considered six priors or hyper-priors for the hyper-parameters of random effects variances $\boldsymbol{\sigma} = (\sigma^2_\omega, \sigma^2_\phi, \sigma^2_{\nu_d}, \sigma^2_{\gamma_d}, \sigma^2_\psi)$ precision parameters $\boldsymbol{\tau} = (\tau_\omega, \tau_\phi, \tau_{\nu_d}, \tau_{\gamma_d}, \tau_\psi)$ used in various literature. Most of these priors are defined using the inverse gamma (IG) distribution [32]. The six priors are

(i) $IG(1, 0.01)$, a specification used in [33];
(ii) $IG(0.001, 0.001)$, the default prior in the BUGS software [34].

(iii) $IG(0.5, 0.0005)$, a specification used in [11];
(iv) $IG(0.01, 0.01)$, a specification used in [16]; and
(v) $\Gamma(1, 0.0005)$, the default specification used in `inla` function of `R-INLA` package [29];
(vi) A half-Cauchy distribution with scale parameter equal to 25, a specification proposed by [35].

We used sensitivity analysis to determine the most appropriate prior for the study data.

To avoid the identifiability problem in the estimation of intercept, in the computation, we enforced a condition that both the sum of the spatial random effects and the sum of temporal random effects equal to zero [11, 26]. The Bayesian hierarchical joint spatiotemporal analyses were conducted using the function `inla()` that is available in the `R-INLA` package [36].

The Deviance Information Criterion (DIC) and conditional predictive ordinates (CPO) were utilised to compare the fitted models. The DIC measures the goodness of fit of a model, and the model with the smallest DIC value is selected as the model that provides the best fit for the data [37]. Whereas the CPO, which is defined as the cross-validated marginal posterior predictive density [38], assesses the predictive capacity of fitted models to the data, where a model with higher CPO value suggests that it has a better predictive performance than other models. However, generally, the CPO value of an observation is close to zero, which was the case in the current study; therefore, the negative sum of cross-validatory predictive log-likelihood [39], i.e., $LS(CPO) = -\sum_{i=1}^{M}\sum_{t=1}^{T}\log CPO_{it}$ where CPO_{it} is the CPO of the ith district at year t, was also used to compare the fitted models for their predictive capacity. Therefore, a model with the lowest $LS(CPO)$ value has the best predictive performance compared to other models.

Ethical consideration

The University of South Africa's School of Science Ethics Committee granted permission for the study (ERC Reference Number: 2021/CSET/SOS/045). Furthermore, the Ethiopian FMoH granted authorization to use their data in the current study. Since we utilised district-level data that have been aggregated, we did not get informed consent from the participants.

Results

Exploratory analysis

Temporal patterns in the number of case notifications for the two diseases are displayed in Fig. 2. Overall, the TB case notifications in Ethiopia slightly decreased from 94,999 in 2015 to 94,713 in 2016 but increased to 96,300 in 2017 and then decreased to 53,675 in 2018. However,

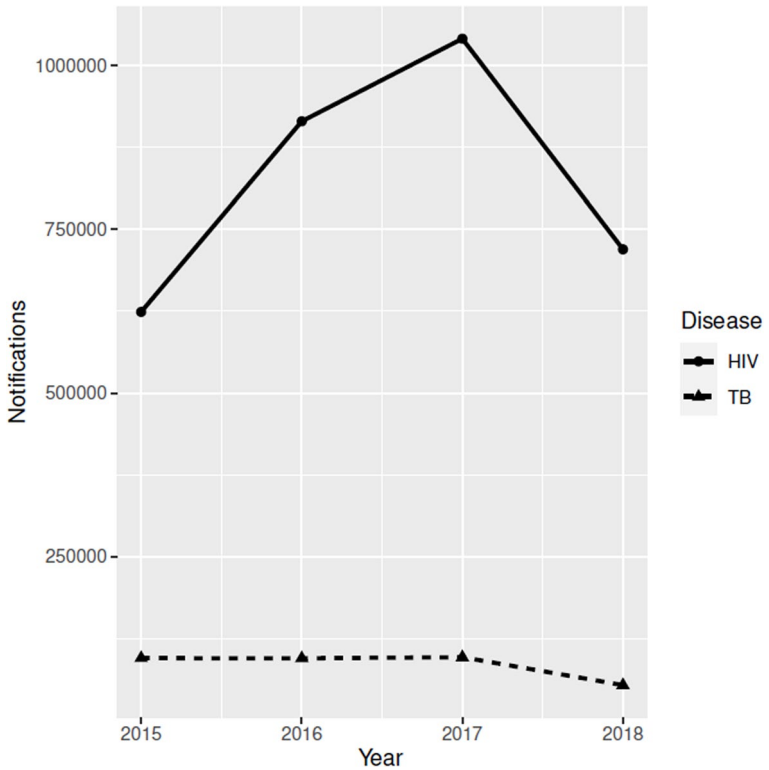

Fig. 2 Temporal patterns in number of HIV and TB case notifications

the number of HIV case notifications registered in HIV health care facilities increased from 623,944 in 2015 to 915,015 in 2016 to 1,041,331 in 2017 and decreased to 719,655 in 2018.

Figure 3, district profile plots, display the temporal trends of case notifications for each disease in all districts. Meanwhile, most districts have shown a constant increase or stability in the number of reported HIV case notifications during the research period. In addition, there is a non-linear pattern seen for other districts in the country, as shown in (see Fig. 3a). However, the number of TB case notifications for quite a large number of districts had a nonlinear pattern (see Fig. 3b). These suggest varying trends in the number of notifications for HIV and TB by district. Therefore, variations in temporal trends among districts can be attributed to disparities in the underlying causal factors and may vary over time.

The correlations among the district raw standardized incidence rates (SIRs) for the two diseases in 2015, 2016, 2017, and 2018 were 0.415, 0.465, 0.372, and 0.487, respectively. All the correlations are statistically highly significant at a 1% significance level. Since the two diseases are related, our proposal of joint spatiotemporal modeling of HIV and TB or an objective of this study was valid.

The mean annual raw HIV SIRs had inconsistency in the trend; it was 1.454, 1.281, 1.473, and 1.431 in 2015, 2016, 2017, and 2018, respectively. However, the raw TB SIRs had a slightly increasing annual trend; it was 1.229, 1.253, 1.300, and 1.337 in 2015, 2016, 2017, and 2018, respectively. To determine the districts with high risks of HIV and TB, we have produced a sequence of maps for raw (unsmoothed) standardized incidence ratio (computed as Observed / Expected) for each disease, and these are displayed in Fig. 4 for HIV and in Fig. 5 for TB. Although, it was observed that the majority of the districts identified as high-risk for HIV between 2015 and 2018 were also classified as high-risk for TB, maps of HIV (Fig. 4) and TB (Fig. 5) displayed varying spatiotemporal patterns. Both diseases seem to have at least one district of high risk in each region and in each city administration, except Harari region, which had a district of high risk for HIV only in 2018. As seen in Figs. 4 and 5, the progression of the risk during the four years 2015–2018 in TB was significantly faster than that of HIV.

Sensitivity analysis

The DIC and $LS(CPO)$ values for each of the six priors of random effects variances precision parameters $\boldsymbol{\tau} = (\tau_\omega, \tau_\phi, \tau_{v_d}, \tau_{\gamma_d}, \tau_\psi)$ used for models fitted to the HIV and TB case notifications data are displayed Table 1. Compared to the DIC values of the other models, the $IG(0.01, 0.01)$, a specification used in [16], had the smallest value, 47695.36. This model also had the lowest $LS(CPO)$ value, 6.97637, and the second lowest $LS(CPO)$, 6.98102, is for the model with the default prior specification used in the `inla` function of `R-INLA` package [29], $\Gamma(1, 0.0005)$. Although the difference between these $LS(CPO)$ values is very small, 0.00465, the difference

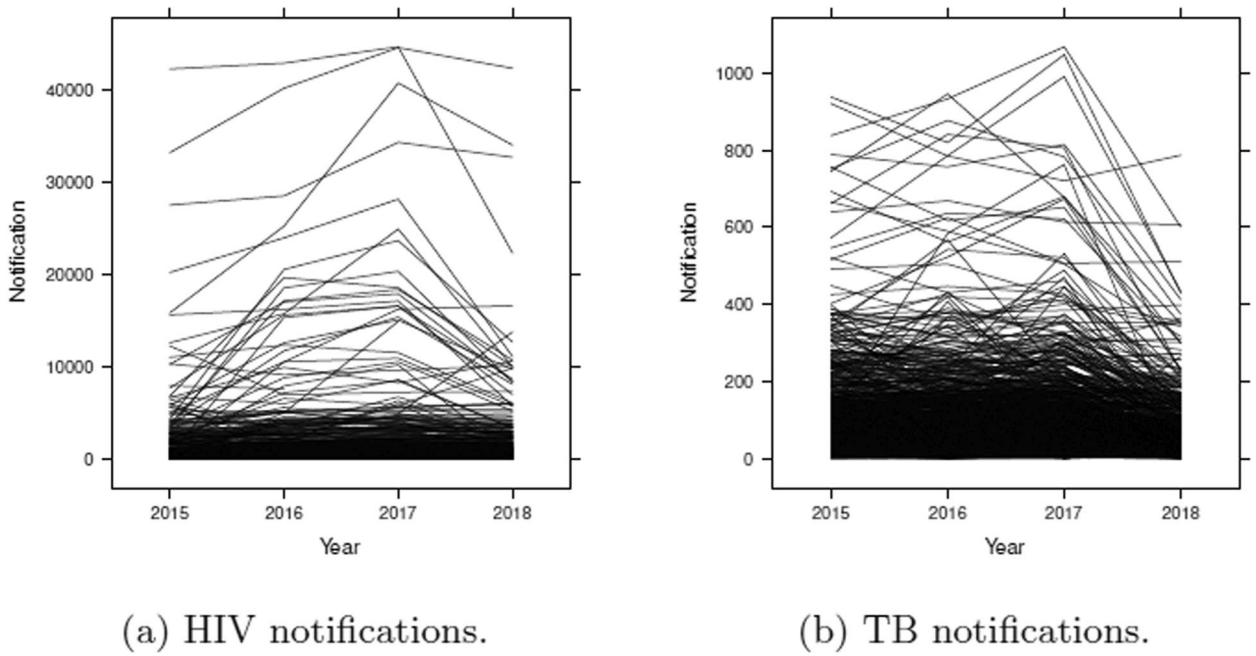

Fig. 3 Districts profile plots for number of HIV (panel **a**) and TB (panel **b**) notifications

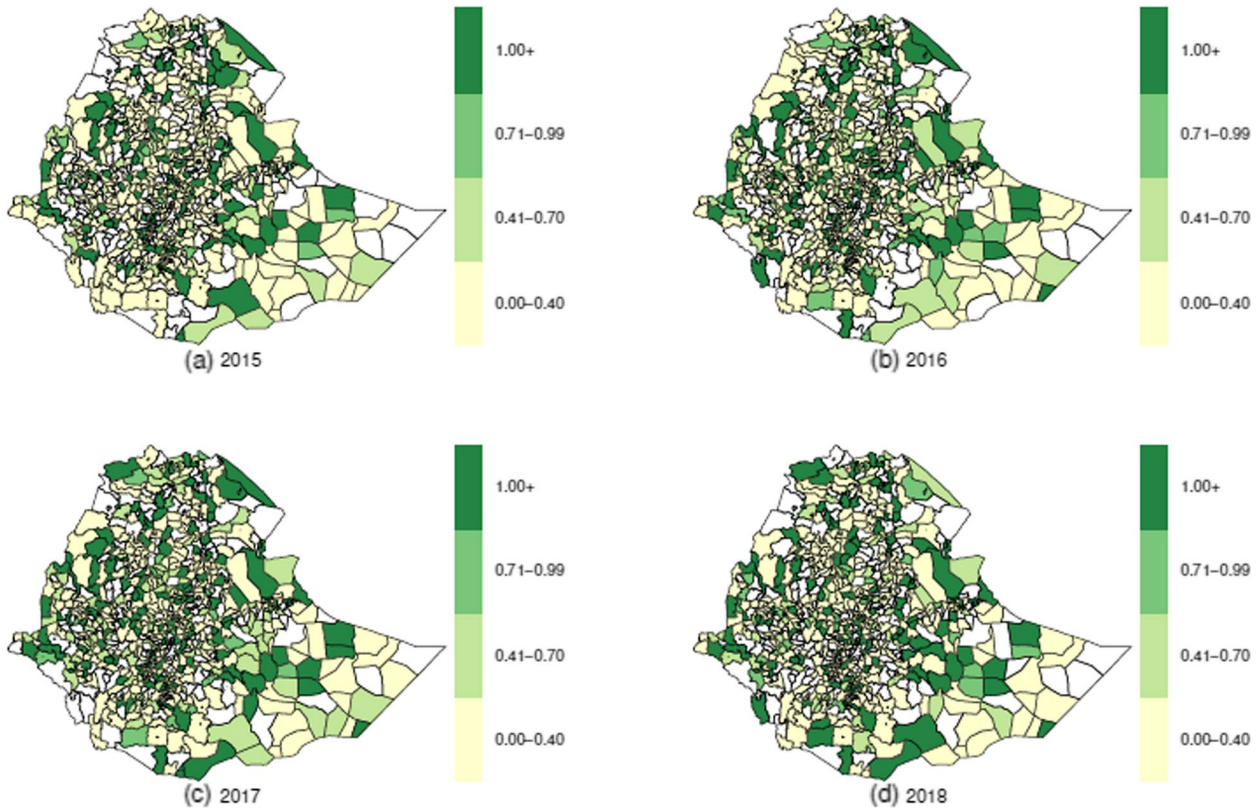

Fig. 4 Standardized incidence ratio for HIV

between their respective DIC values, 7.32, is greater than five, hence, it is a substantial difference [37]. Therefore, the model with the $IG(0.01, 0.01)$ prior provided the best fit for the data and had the best predictive performance. Thus, in the sections that follow, we only present findings from model in Expression (1) with $IG(0.01, 0.01)$ prior.

The estimated posterior means and the credible intervals (CI) of disease-specific intercepts, derived from the selected prior, are summarised in Table 2. Additionally, the precision parameters of shared and disease-specific spatial and temporal random effects, as well as the interaction random effect of space and time, are presented in Table 2. The table also contains the proportion (percent) variation in the model explained by each random effect. The findings from the chosen model indicate that approximately 53% of the variation in HIV and TB incidences during the study period can be accounted for by the combined influence of the shared temporal component, the disease-specific spatial effect of HIV, and the interaction effect of space and time.

The posterior means for the coefficients of shared spatial patterns of the two diseases are distinct from one another, and the 95% credible intervals show that the weight of HIV is significantly higher than one. The latter suggests that HIV is more dependent on the shared spatial patterns, hence its spatial pattern closely resembles the shared pattern. The results show that the shared temporal random effect, HIV disease-specific spatial random effect, and the random interaction effect between space and time explain most of the variability in the respective order. The variations explained by HIV disease-specific spatial random effect and temporal random effect are higher than those of TB (Table 2).

Spatial analysis

The relative risk related to the combined spatial patterns for HIV and TB, calculated from the posterior means of total spatial effect, i.e., $\exp(\omega_i + \nu_{di})$, are displayed in Fig. 6. The two diseases show similar spatial patterns in the two city administrations and in some districts, such as at the Western and Eastern Tigray region, Kilbert Raisu (Zone 2) of the Afar region, Central and North Gondar zones in the Amhara region, Asosa zone in the Benishangul-Gomuz region, Anuak zone in the Gambela region, Borena zone in the Oromiya region, Sitti zone in the Somali region including boarder areas in Liben and Shabelle zones in the Somali region.

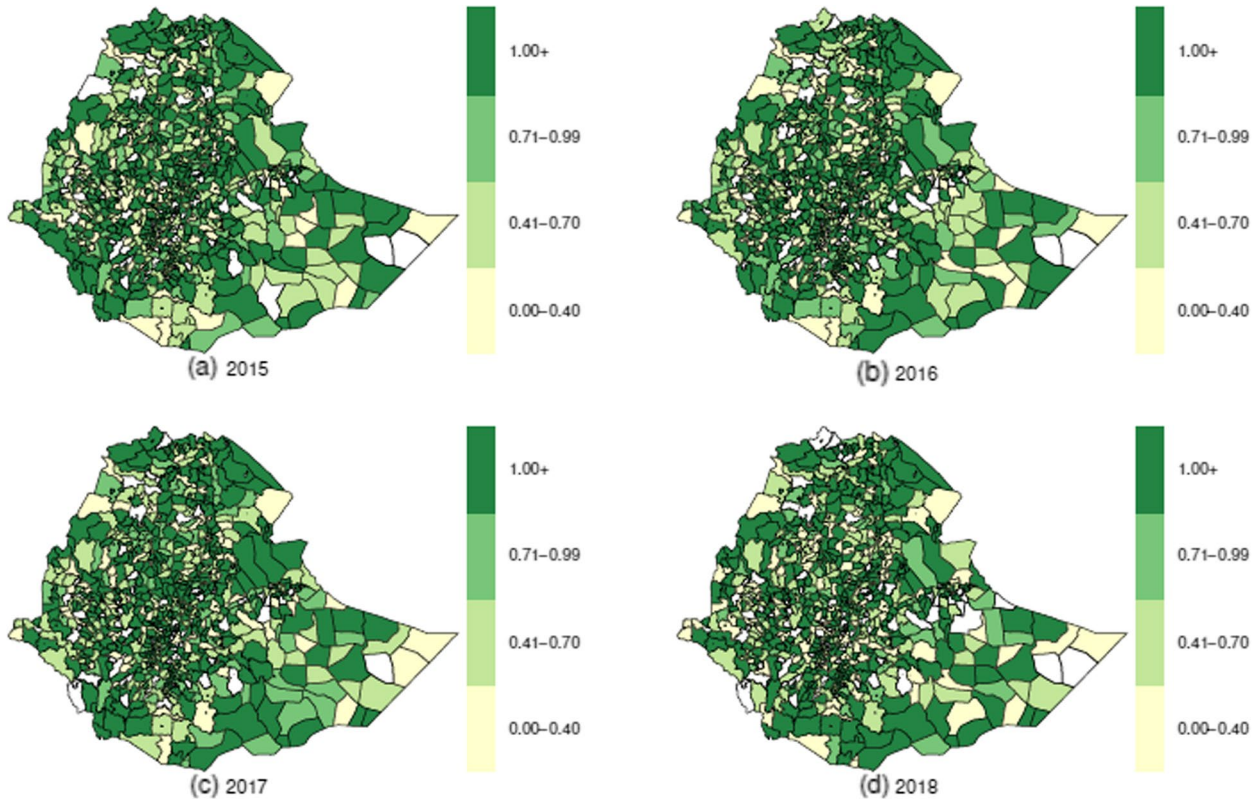

Fig. 5 Standardized incidence ratio for TB

Table 1 Summary of DIC and *LS*(*CPO*) values of models included in sensitivity analysis

	Type of prior					
	***IG*(1, 0.01)**	***IG*(0.001, 0.001)**	***IG*(0.5, 0.0005)**	***IG*(0.01, 0.01)**	***IG*(1, 0.0005)**	**Half-Cauchy**
DIC	47698.69	47698.94	47699.76	47695.36	47702.68	47699.81
LS(*CPO*)	6.98187	6.99771	6.99738	6.97637	6.98102	6.98175

There were districts identified as high-risk areas within the two city administrations, within all zones of the Afar region; within Awi, east Gojjam, north Gondar, north and south Wollo, and north Shewa zones in the Amhara region; within Asosa and Kemashi zones in the Benishangul-Gumuz region; within Anuak, Mezhenger and Nuer zones in the Gambella region; within the Harari region, Arsi, east Hararge, Horo Guduru Wollega, Illubabor, Jimma, north Shewa and west Shewa zones in the Oromiya region; within Bench Maji, Gamo Gofa, Gurage, Hadiya, Keffa, Sidama and Wolayta zones in the SNNP region; within Nogob and Shebele zones in the Somali region; and central and east Tigray zones in the Tigray region.

The TB high-risk districts most of them were overlap with the HIV high-risk districts, but in some regions, they were different. The districts that are at a high risk of TB were in the two city administrations, in all zones of the Afar region; in east Gojjam, south Wollo, north Gondar and north Shewa zones in the Amhara region; in Kemashi and Metekel zones in the Benishangul-Gumuz region; in Anuak zone in the Gambella region, the Harari region, Arsi, Bale, east Wellega, Finfine zuria, Ilu Aba Bora, Jimma and north Shewa, west Hararge, and west Shewa zones in the Oromiya region; Bench Maji, Gamo Gofa, Gurage, Keffa, Sidama, south Omo and Wolayta zones in the SNNP region; in Afder, Gode and Shinle zones in the Somali region, and central, northwest and south Tigray zones in the Tigray region.

Figure 7 shows the relative risks for the shared spatial effect ($\exp(\omega_i)$) and disease-specific spatial effects ($\exp(\nu_{di})$) patterns. In the three maps, there were common districts of high risk within each region and the two city administrations. On the other hand, when compared

Table 2 Summary statistics for estimates of the precision parameters of random effects and coefficients for shared spatial and temporal effects

Parameter	Estimates		
	Mean	95% CI	Percentage of variation
Fixed effect			
α_1	−1.529	(−1.591, −1.466)	
α_2	−0.134	(−0.153, −0.114)	
Precision parameter			
τ_ω	1.133	(1.046, 1.212)	13.0
τ_ϕ	1.776	(1.253, 2.631)	20.5
τ_{ν_1}	1.550	(1.439, 1.749)	17.9
τ_{ν_2}	0.976	(0.926, 1.017)	11.2
τ_{γ_1}	1.200	(1.060, 1.460)	13.8
τ_{γ_2}	0.807	(0.680, 1.032)	9.3
τ_ψ	1.239	(1.170, 1.505)	14.3
Coefficients for Shared Spatial effect			
δ_{HIV}	3.300	(3.042, 3.556)	
δ_{TB}	0.847	(0.736, 0.936)	
Shared Temporal effect			
κ_{HIV}	0.964	(0.199, 2.656)	
κ_{TB}	0.582	(0.060, 1.888)	

to TB disease-specific spatial patterns, the number of districts with a high relative risk (> 1.0) of HIV disease-specific spatial patterns is higher, followed by the number of districts with a high relative risk (> 1.0) of shared spatial patterns. This may be because HIV is more dependent on the shared spatial term, which means that the shared pattern explains most of the HIV disease-specific patterns. The presence of shared spatial variation or clustering depicted in Fig. 7a can be interpreted as a surrogate for covariates that exhibit spatial variation not included in the model but shared with both diseases [27].

Temporal analysis

The relative risks associated with the shared temporal random effect $\exp(\phi_t)$, disease-specific temporal random effects $\exp(\gamma_{dt})$, and the shared trend effect $\exp(\phi_t + \gamma_{dt})$ are depicted in Fig. 8. The shared temporal random effect suggests a slight increase in risk from 2015 to 2017, then a decrease in risk in 2018. The estimated values of risks are in the interval [0.808, 1.165]. HIV disease-specific temporal effect does not deviate from the shared temporal pattern (its values range between 0.773 and 1.177). However, the specific temporal pattern for TB has a relative risk close to one for the study period (its value ranges between 0.947 and 1.102). The plots in Fig. 8 show that the shared temporal effect almost captures the increasing trend in HIV risk for the first three study years and then a decreasing trend in 2018, whereas the specific effect is negligible because the relative risk estimates are very close to one for all years.

Similar to the shared temporal random effect and HIV disease-specific temporal trend, the combined temporal trend for HIV showed an initial increase in risk over the first three years and then a decreasing trend for 2018 (its values range between 0.653 and 1.293), while the combined temporal trend of TB was almost constant at 1 over the study period (its values range between 0.990 and 1.022). Based on the case notification data, the relative risk of HIV had an increasing trend between 2016 and 2018, and this risk was generally higher compared to the relative risk of TB within the same period.

Table 2 also displays summary statistics of weights κ_d, $d = 1, 2$ for the shared temporal trend. The weight for HIV ($\kappa_1 = 0.964$) was higher than that of TB ($\kappa_2 = 0.582$). Since the weight for HIV is very close to

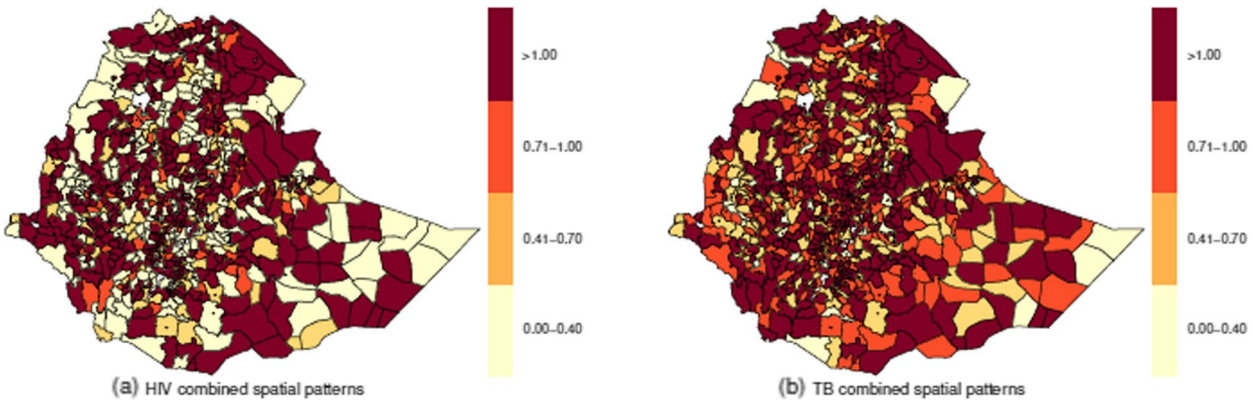

Fig. 6 Posterior means of the total spatial effect of HIV (left panel) and TB (right panel)

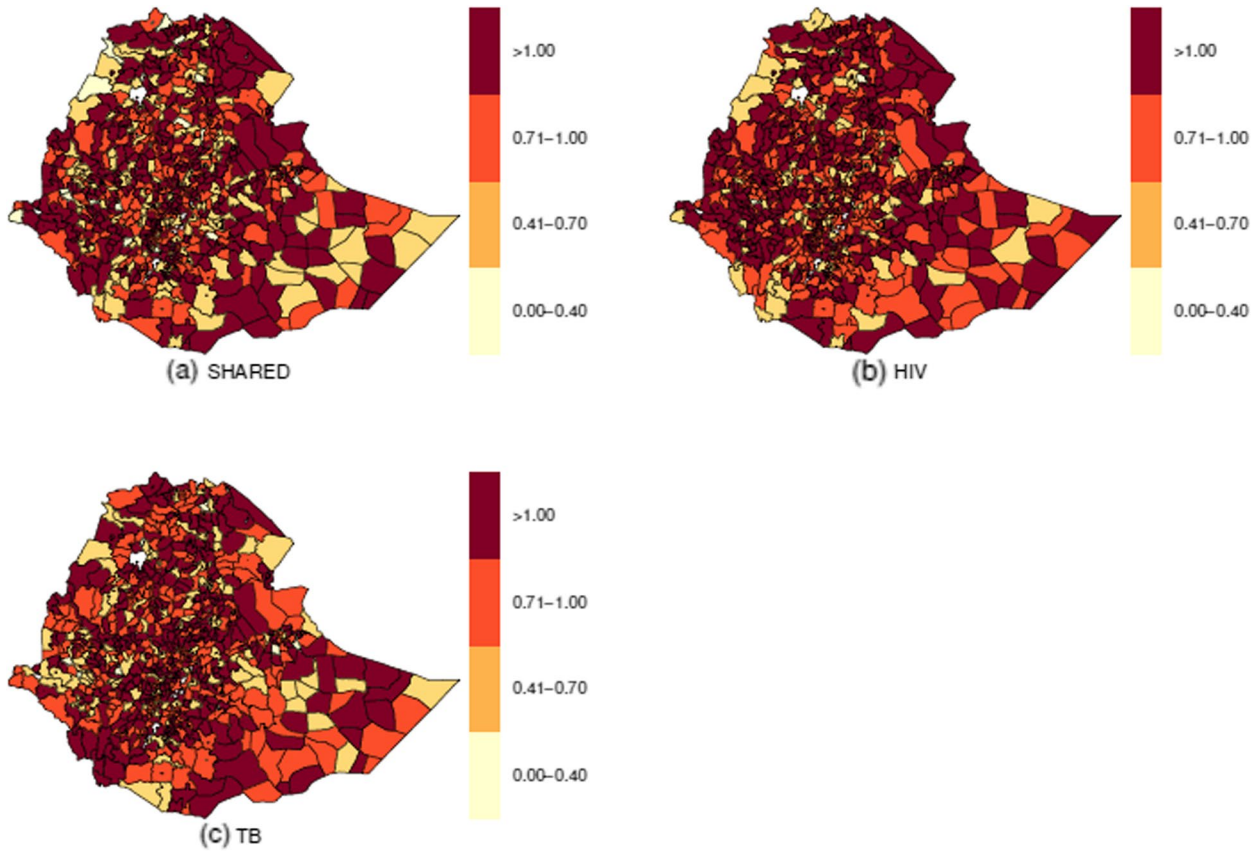

Fig. 7 Relative risk of shared spatial patterns (ω_i) and disease specific spatial patterns (ν_{di})

one, this suggests that this disease had a strong dependence on the shared temporal pattern.

Joint spatiotemporal analysis

To identify districts with the most substantial space-time interactions, we have produced a map highlighting districts with posterior probabilities of exhibiting a relative risk greater than one (exceedance relative risk) for the smoothed joint spatiotemporal interaction for each study period in Fig. 9. In the figure, if the posterior probability of a district is within the interval [0.81, 1.00], then it is counted as a high-risk area for a disease (HIV or TB) [40]. The number of districts per region with posterior probabilities within the interval [0.81, 1.00] varies between 0 and 21 in 2015 (0 districts in the Benishengul-Gumuz and Harari regions and 21 districts in the Oromia region); between 0 and 14 in 2016 (0 districts in the Afar, Benishengul-Gumuz, Gembella and Harari regions, and 14 districts in the Oromia region); between 0 and 16 in 2017 (0 districts in the two city administrations, Afar, Benishengul-Gumuz, Gambella and Harari regions, and 16 districts in the Oromia region), and between 0 and 11 in 2018 (0 districts in the two city administrations, Benishengul-Gumuz, Gambella, and Harari regions, and 11 districts in the Oromia region). The country had 58, 32, 43, and 27 such districts in 2015, 2016, 2017, and 2018, respectively.

In 2015, relatively more districts with high risks were noticed in east and west Gojjam, south Gondar and south Wollo zones in the Amhara region, Bale, west Hararge, west Shoa and west Wollega zones in the Oromiya region, Gurage zone in SNNP region, east and northwest Tigray zones in the Tigray region. Similarly, in 2016, such districts were observed in north and south Wollo zones in the Amhara region, north and west Shoa, east and west Wollega zones in the Oromiya region; in 2017, north and south Wollo, and north Shewa zones in the Amhara region, east Hararge and west Shoa zones in the Orpmiya region, and central and south Tigray zones in the Tigray region; whereas in 2018, in west Shoa zone in the Oromiya region and Gamo Goffa zone in the SNNP region.

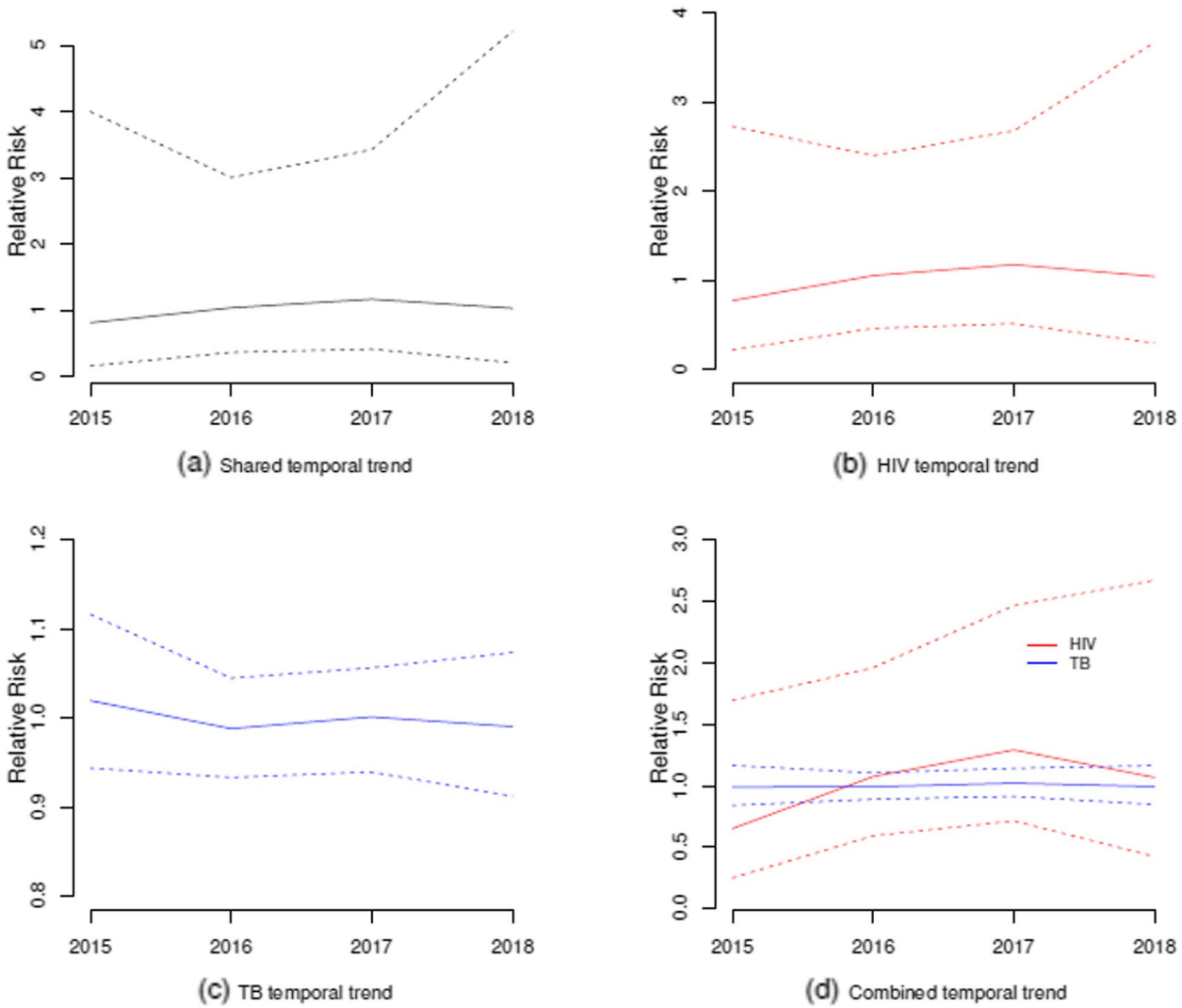

Fig. 8 Relative risks of shared temporal effect $\exp(\phi_t)$ (**a**), disease-specific temporal effects $\exp(\gamma_{dt})$ (**b**, **c**) and total temporal effect $\exp(\phi_t + \gamma_{dt})$ (**d**)

Discussion

Although WHO-coordinated initiatives have made progress, HIV and TB diseases still have alarming rates of illness and mortality [41]. In the current study, we assessed the joint spatiotemporal variation of HIV and TB risks at the district levels for four years, from 2015 to 2018, in Ethiopia by jointly analyzing data on the two diseases obtained from HMIS. Using a Bayesian hierarchical model, we were able to characterize the spatial and temporal patterns that are shared and disease-specific, as well as the space-time interaction effects of HIV and TB relative risks. It also enabled us to estimate the relative risks of both shared and disease-specific risks, as well as the interaction of space and time effects, and to display these estimates over all the districts in the country.

Results from the exploratory analysis showed that there had been an increase in HIV case notifications registered in HIV healthcare facilities between 2015 and 2017, but there was a sharp decrease from 2017 to 2018; this could be because about 25% of districts failed to submit the HIV case notifications to the national Health Management Information System in 2018. However, TB case notifications had inconsistencies in the annual trend. While the mean raw yearly TB SIRs showed a slightly increasing trend, the raw HIV SIRs showed an inconsistency in the yearly trend. The results also showed that most of the districts identified as high risk for HIV during the study period were also classified as high risk for TB; however, each disease had spatiotemporal variation in the raw relative risk in the four-year study period, 2015–2018. This finding agrees with the FDREMH 2018 report [42]. Except for the Harari region, which had

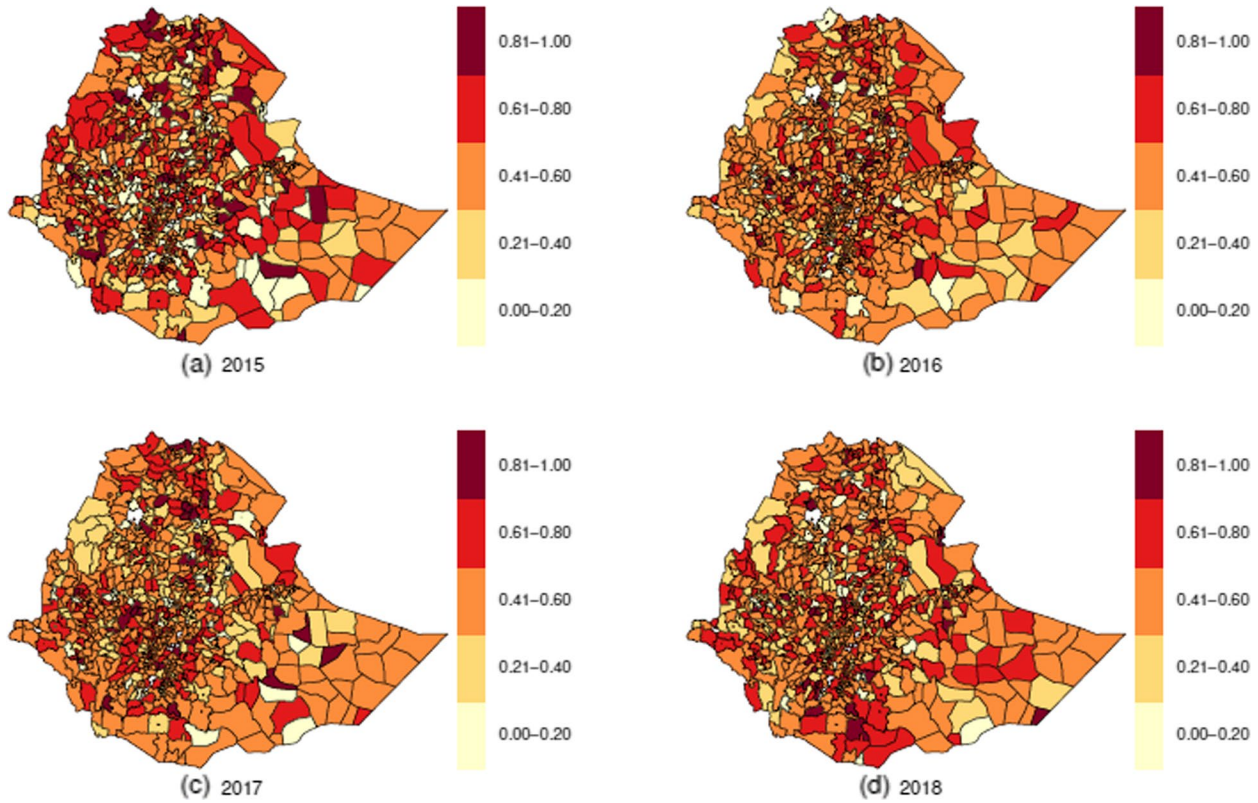

Fig. 9 Posterior probabilities of having an estimation of the common space-time interaction term relative risk $\exp(\psi_{it})$ greater than 1, i.e. $P(\exp(\psi_{it}) > 1|\mathbf{y})$ for each study period

one district of high risk for HIV in 2018, both diseases had at least one district of high risk in each region and in each city administration. There were low reported TB and HIV case notifications in some districts, specifically in the Somali region. Despite the national guidelines recommendation to offer HIV testing to those patients with presumptive TB, there is lag in tracking its implementation in some parts of the country. Therefore, the government may need to implement intensified community-based TB and HIV tests, routine contact investigations, and targeted population-focused interventions.

Overall, the geographic spread of HIV in proportion to TB was more extensive. These findings agree with the results of [43], which indicate that HIV has surpassed TB to a large extent in Mauritania, Senegal, and Gambia. However, the results of the present investigation diverge from those of previous studies in Kenya [26, 44] and [43], which also revealed that TB seemed to be spreading more rapidly than HIV in Rwanda and Burundi. In most districts, the spatial patterns observed in the unsmoothed maps of SIRs for both diseases remained consistent with the spatial patterns of smoothed relative risks. Nevertheless, there were cases where the concentration of high incidence districts became less apparent, for example, for HIV SIR's districts in the northern part of Fanti Rasu zone (Zone 4) in the Afar region and districts in the south part of Itang zone in the Gambela region in 2015.

In this study, the shared temporal trend showed a marginal increase in risk from 2015 to 2017, followed by a modest decline in 2018. HIV disease-specific temporal pattern had a similar trend to the shared temporal trend. On the other hand, the temporal pattern of tuberculosis risk that was particular to the disease exhibited a level of consistency that was nearly constant throughout the study period. Like the shared and specific temporal trend of HIV, the combined temporal trend for HIV also had a rising risk for the first three years and then a decreasing trend for 2018, while the combined temporal trend of TB was almost constant at 1 over the study period. The case notifications data show that compared to the risk of TB, the temporal trend of the risk of HIV was lower in the year 2015. However, the risk of HIV trend exceeded that of TB over the period 2016 to 2018. These findings agree with the observations made by [44], where in their study, the researchers observed that the rate of HIV risk had a reduced magnitude compared to that of TB during the first two years, but in the last three years, the HIV risk surpassed the TB risk. Although HIV drives TB-related

infections, the lower or constant trend of TB in the country during the study period could be due to the government's effort that all eligible HIV-positive people in areas with a high prevalence of TB should receive TB preventive medication before developing severe manifestations of the virus. Studies in Ethiopia [45, 46] demonstrate this. Other studies in Sub-Saharan Africa also observed similar temporal patterns in TB incidences [47, 48].

There were 174 (22%) districts with similarities in HIV spatial distribution and tuberculosis in the country from 2015 to 2018. Of these districts, 59, 34, 29, 13, and 11 were in the Oromia, SNNP, Amhara, Afar, and Somali regions. The least number of such districts was observed in the Harari region and the Dire Dawa city administration; each had one district. Addis Ababa city administration and the Gambella region had four districts, while the Benishangul-Gumuz and Tigray regions had nine such districts. The large number of districts with high risks of HIV and TB suggests that these districts have inadequate HIV and TB control. If no efficient interventions are developed and implemented, these districts may remain a source of HIV and TB spread. In contrast to the distribution of HIV, which had many districts classified as high-risk areas, the distribution of the shared relative risks was comparable to the distribution of the disease-specific relative risk for tuberculosis. This similarity may be due to a greater dependence on the shared spatial component of HIV, meaning that the HIV spatial patterns are responsible for most of the shared components.

Recall that these two components also had similar temporal trends over the study period. Our results differ from those of [44], whose findings show that there was only a slight difference between the disease-specific risk of HIV and the distribution of the shared risks. However, the distribution of tuberculosis showed a significantly higher number of counties classified as high-risk locations. In addition, other studies in Uganda [44] and China [49] observed the regional clustering of tuberculosis and HIV. However, they applied a co-clustering approach. In the former, the results also show the combined co-clustering of the two diseases. Studies in Brazil reported spatial clustering and temporal trends of HIV incidence [50]. Analyses of spatiotemporal trends of HIV incidence/prevalence in other countries have also demonstrated that the spread of HIV infection varies in both space and time [51, 52].

The posterior probabilities of having an exceedance relative risk for the smoothed joint spatiotemporal interaction were computed for each district and mapped for each study period to identify districts having the most significant spatiotemporal interactions. The results show that interaction components are more prevalent in districts with a relative risk higher than one, suggesting that other factors could play a role in these districts. However, the exceedance risk was consistent around the north and south Wollo zones in the Amhara region, north Shoa, west Shoa, and west Wollega in the Oromia region over most of the study years. Studies conducted in China [49] and Brazil [53] also demonstrated a substantial correlation between the joint risks of both diseases using bivariate maps for the joint distribution of HIV and TB. Furthermore, the findings from the study conducted in Brazil revealed that both diseases are spatially heterogeneous across the country.

Investigating relationships between diseases and geographic space over time is essential to elucidate the extent and severity of the infection and its impact on public health. Such assessment helps to identify priority areas that need control interventions. The effectiveness of infectious disease control efforts is maximized when locations with high rates of reported cases are identified and thoroughly documented. Furthermore, to design highly efficient strategies aimed at decreasing the rates of tuberculosis and HIV transmission, conducting a thorough evaluation of the combined epidemiological patterns of incidences for both diseases, at least at the district level over time. Implementing efficient control measures in regions characterized by a significant likelihood of contracting HIV and TB leads to successful containment of the pandemic [54]. Furthermore, an extensive understanding of high-risk regions is crucial for the effective implementation of surveillance programs and the efficient allocation of resources [55].

Although statistical methods for spatiotemporal analysis of several diseases are well developed, based on the authors' knowledge, this is the first research on the joint spatiotemporal modeling of HIV and TB incidence notifications data using a Bayesian hierarchical approach in Ethiopia. However, our findings might have been influenced by the following limitations:

(1) In the current paper, we used HIV and TB case notification data as a proxy to represent people living with HIV and TB. These data are obtained from subgroups of people who seek medical treatment and care from local healthcare facilities. Therefore, they are indicative of the population residing in the vicinity of these facilities.
(2) Since we utilized district-level consolidated data in the study, the conclusions drawn cannot be extrapolated to smaller administrative units in the country, such as Kebele or household levels.
(3) It is essential to note that the data on HIV and TB case notifications obtained from the national HMIS may not provide an accurate depiction of the actual prevalence of these diseases in a specific district.

This discrepancy could be attributed to cases being underreported or not properly detected.

(4) The spatial variations or clustering of the two diseases may be due to different factors not included in the model due to data limitations. However, as stated in the previous section, the shared spatial and temporal components can be interpreted as surrogates for covariates that exhibit spatial and temporal patterns not included in the model but shared with both diseases [27]. At the same time, each disease-specific spatial and temporal component represents those spatially varying and have temporal patterns of risk factors specific to the disease. However, conducting further research that considers additional covariates would be beneficial in exploring the underlying causes of district-level variations. This can be achieved using the joint Bayesian spatiotemporal generalized linear models to examine potential risk factors for TB and HIV infections.

Conclusion

This paper assessed the joint spatial clustering of HIV and tuberculosis incidence in Ethiopian districts and how they vary over four years, 2015–2018. The Bayesian hierarchical joint spatiotemporal models with shared spatial and temporal random effects, disease-specific spatial and temporal random effects, and interaction between space and time random effect were applied for the analysis. The models allowed borrowing strength across both districts, years, and between diseases to produce smoothed district-level HIV and TB incidence estimates separately for each disease and jointly.

The selected model enabled us to cluster districts that had a high probability of contracting HIV and TB. Overall, the study facilitated the identification of districts with a significant likelihood of contracting HIV and TB, making them a top target for control actions. Moreover, the results of this study could offer Ethiopian health policymakers significant insights for enhancing national, regional, zone, and district strategies in addressing area-specific and comprehensive TB and HIV/AIDS collaborative efforts, as well as in strengthening measures to prevent infection of HIV and TB.

Supplementary Information

The online version contains supplementary material available at https://doi.org/10.1186/s12889-024-20996-7.

Supplementary Material 1. The R code used for the analysis is available as supplementary material in the "Supplementary Material 1" file.

Acknowledgements
We express our gratitude to the Ethiopian Ministry of Health Office for permitting us to use the data. Furthermore, the co-author expresses his gratitude for the financial assistance provided by the National Research Foundation of South Africa and the University of South Africa in support of his doctoral research.

Authors' contributions
Both authors conceptualized the statistical methods employed in the study; the L.L.G. conducted the analyses and drafted the manuscript; L.K.D. reviewed the findings of data analyses and the writing of the manuscript. Both writers gave their consent to the final manuscript.

Funding
Open access funding provided by University of South Africa. No financial assistance was received either to conduct the research or for the preparation of the article.

Data availability
The data that support the findings of this study are available from Ethiopian Ministry of Health Office but restrictions apply to the availability of these data, which were used under license for the current study, and so are not publicly available. Data are however available from the authors upon reasonable request and with permission of Ethiopian Ministry of Health Office.

Declarations

Ethics approval and consent to participate
Ethical approval to conduct the study was obtained from the School of Science Ethics Committee, University of South, South Africa. Since we utilised district-level data that have been aggregated, we did not get informed consent from the participants, and this was approved by the University of South Africa's School of Science Ethics Committee (ERC Reference Number: 2021/CSET/SOS/045).

Consent for publication
Not applicable.

Competing interests
The authors declare no competing interests.

Author details
[1]Department of Statistics, University of South Africa, c/o Christiaan de Wet Road & Pioneer Avenue, Private Bag X6, Florida, 1710 Johannesburg, South Africa.

Received: 15 June 2024 Accepted: 5 December 2024
Published online: 30 January 2025

References

1. De Cock KM, Chaisson RE. Will DOTS do it? A reappraisal of tuberculosis control in countries with high rates of HIV infection. Int J Tuberc Lung Dis. 1999;3:457–65.
2. Dahle UR. Extensively drug resistant tuberculosis: beware patients lost to follow-up. BMJ. 2006;333(7570):704–6. https://doi.org/10.1136/bmj.333.7570.705.
3. Ramkissoon S, Mwambi HG, Alan P. Modelling HIV and MTB co-infection including combined treatment strategies. PLOS ONE. 2012;169(2):321–54. https://doi.org/10.1371/journal.pone.0049492.
4. Ethiopian Public Health Institute (EPHI). Ethiopia Population-based HIV Impact Assessment (EPHIA) 2017-2018: Final Report. 2020. Figshare https://www.who.int/news-room/fact-sheets/detail/hiv-aids. Accessed 2 June 2022.
5. Raviglione MC. Tuberculosis: the essentials. 4th ed. New York: CRC Press; 2016.
6. World Health Organization. Global tuberculosis report 2018. 2018. Figshare https://apps.who.int/iris/handle/10665/274453. Accessed 2 June 2022.

7. Belay M, Bjune G, Abebe F. Prevalence of tuberculosis, HIV, and TB-HIV co-infection among pulmonary tuberculosis suspects in a predominantly pastoralist area, northeast Ethiopia. Glob Health Action. 2015;8(27949). https://doi.org/10.3402/gha.v8.27949.
8. World Health Organization. Guide to Monitoring and Evaluation for Collaborative TB/HIV Activities-2015. 2015. Figshare https://iris.who.int/bitstream/handle/10665/150627/9789241508278_eng.pdf?sequence=1. Accessed 2 June 2022.
9. World Health Organization. HIV-Associated Tuberculosis: factsheet (2021). 2021. Figshare https://www.who.int/tb/areas-of-work/tb-hiv/tbhivfactsheet.pdf?ua=1. Accessed 2 June 2022.
10. Martínez-Beneito MA, Botella-Rocamora P. Disease Mapping: from Foundations to Multidimensional Modeling. New York: CRC Press; 2019.
11. Richardson S, Abellan JJ, Best N. Bayesian spatio-temporal analysis of joint patterns of male and female lung cancer risks in Yorkshire (UK). Stat Methods Med Res. 2006;15(4):385–407. https://doi.org/10.1191/0962280206sm458oa.
12. Knorr-Held L. Bayesian modelling of inseparable space-time variation in disease risk. Stat Med. 2006;19(17–18):2555–67. https://doi.org/10.1002/1097-0258(20000915/30).
13. Dabney AR, Wakefield JC. Issues in the mapping of two diseases. Stat Methods Med Res. 2005;14(1):83–112. https://doi.org/10.1191/0962280205sm340oa.
14. Kim H, Sun D, Tsutakawa RK. A bivariate bayes method for improving the estimates of mortality rates with a twofold conditional autoregressive model. J Am Stat Assoc. 2001;96(456):1506–21.
15. Tzala E, Best N. Bayesian latent variable modelling of multivariate spatio-temporal variation in cancer mortality. Stat Methods Med Res. 2008;17(1):97–118. https://doi.org/10.1177/0962280207081243.
16. Gómez-Rubio V, Palmí-Perales F. Multivariate posterior inference for spatial models with the integrated nested Laplace approximation. J R Stat Soc Ser C (Appl Stat). 2019;68(1):199–215. https://doi.org/10.1111/rssc.12292.
17. Chidumwa G, Maposa I, Kowal P, Micklesfield LK, Ware LJ. Bivariate Joint Spatial Modeling to Identify Shared Risk Patterns of Hypertension and Diabetes in South Africa: Evidence from WHO SAGE South Africa Wave 2. Int J Environ Res Public Health. 2021;5(18):1–12. https://doi.org/10.3390/ijerph18010359.
18. Dangisso MH, Datiko DG, Lindtjørn B. Spatio-temporal analysis of smear-positive tuberculosis in the Sidama Zone, southern Ethiopia. PLoS ONE. 2015;10(6). https://doi.org/10.1371/journal.pone.0126369.t004.
19. Alene KA, Viney K, McBryde ES, et al. Spatiotemporal transmission and socio-climatic factors related to paediatric tuberculosis in north-western Ethiopia. Geospatial Health. 2017;12(575):342–50. https://doi.org/10.1371/journal.pone.0226127.
20. Gelaw YA, Magalhães RJ, Y A, Williams G. Spatial clustering and socio-demographic determinants of HIV infection in Ethiopia, 2015-2017. Int J Infect Dis. 2019;82:33–39. https://doi.org/10.1016/j.ijid.2019.02.046.
21. Kibret GD, Ferede A, Leshargie CT, Wagnew F, Ketema DB, Alebel A. Trends and spatial distributions of hiv prevalence in Ethiopia. Infect Dis Poverty. 2019;8(1):1–9. https://doi.org/10.1186/s40249-019-0594-9.
22. Sebu AT, Genati KT, Bekalo DB, Deressa TK. Spatiotemporal dynamics of tuberculosis in East Hararge zone, Oromiya region, Ethiopia. Spat Inf Res. 2020;28(6):623–33. https://doi.org/10.1007/s41324-020-00319-9.
23. Asemahagn MA, Alene GD, Yimer SA. Spatial-temporal clustering of notified pulmonary tuberculosis and its predictors in east Gojjam zone, northwest Ethiopia. PLoS ONE. 2021;16(1). https://doi.org/10.1371/journal.pone.0245378.
24. Belay H, Azim T, Kassahun H. Assessment of health management information system (HMIS) performance in SNNPR, Ethiopia USAID Measure Evaluation, SNNP Regional Health Bureau: Washington, DC, USA. 2013. Figshare https://www.measureevaluation.org/publications/sr-14-87. Accessed 2 June 2022.
25. Tadesse K, Gebeyoh E, Tadesse G. Assessment of health management information system implementation in Ayder referral hospital, Mekelle, Ethiopia. Int J Intell Inf Syst. 2014;3(4):34–9. https://doi.org/10.1371/journal.pone.0226127.
26. Otiende V, Achia T, Mwambi H. Bayesian modeling of spatiotemporal patterns of TB-HIV co-infection risk in Kenya. BMC Infect Dis. 2019;19(902). https://doi.org/10.1186/s12879-019-4540-z.
27. Knorr-Held L, Best NG. A shared component model for detecting joint and selective clustering of two diseases. J R Stat Soc Ser A (Stat Soc). 2001;164(1):73–85. https://doi.org/10.1111/1467-985X.00187.
28. Gilks WR, Spiegelhalter DJ, Richardson S. Generalised Linear Mixed Models. London: Chapman & Hall; 1996.
29. Rue H, Martino S, Chopin N. Approximate Bayesian Inference for Latent Gaussian models using Integrated Nested Laplace Approximations. JRSS Series B. 2009;71(2):319–92. https://doi.org/10.1111/j.1467-9868.2008.00700.x.
30. Gemechu LL, Debusho LK. Bayesian spatial modelling of tuberculosis-HIV co-infection in Ethiopia. PLoS ONE. 2023;18(3). https://doi.org/10.1371/journal.pone.0283334.
31. Rubio VG, Perales FP, Abente GL, Rebeca Ramis-Prieto RR, Navarro PF. Bayesian joint spatio-temporal analysis of multiple diseases. SORT. 2019;43(1):51–74. https://doi.org/10.2436/20.8080.02.79.
32. Grilli L, Metelli S, Rampichini C. Bayesian estimation with integrated nested laplace approximation for binary logit mixed models. J Stat Comput Simul. 2009;85(13):2718–26. https://doi.org/10.1080/00949655.2014.935377.
33. Baker J, White N, Mengersen K, Rolfe M, Morgan GG. Joint modelling of potentially avoidable hospitalisation for five diseases accounting for spatiotemporal effects: A case study in new South Wales, Australia. PLoS One. 2017;12(8). https://doi.org/10.1371/journal.pone.0183653.
34. Lunn JCD, Best N, Thomas A. The BUGS Book: A Practical Introduction to Bayesian Analysis. New York: CRC Press; 2012.
35. Gelman A. Prior distributions for variance parameters in hierarchical models (comment on article by browne and draper). Bayesian Anal. 2006;1(3):515–34. https://doi.org/10.1214/06-BA117A.
36. Rue H, Riebler A, Sørbye SH, Illian JB, Simpson DP, Lindgren FK. Bayesian computing with INLA: a review. Ann Rev Stat Appl. 2017;4:395–421. https://doi.org/10.1146/annurev-statistics-060116-054045.
37. Spiegelhalter DJ, Best NG, Carlin PB, van der Linde A. Bayesian measures of model complexity and fit. J R Stat Soc Ser B. 2002;64(4):583–639. https://doi.org/10.1111/1467-9868.00353.
38. Dey D, Chen MH, Chang H. Bayesian approach for nonlinear random effects models. Biometrics. 1997;53(4):1239–52. https://doi.org/10.2307/2533493.
39. Gneiting T, Raftery AE. Strictly Proper Scoring Rules, Prediction, and Estimation. J Am Stat Assoc. 2007;102(477):359–78. https://doi.org/10.1198/016214506000001437.
40. Blangiardo M, Cameletti M. Disease Mapping: from Foundations to Multidimensional Modeling. United Kingdom: Wiley; 2015.
41. UNAIDS. United Nations Programme on HIV/AIDS (UNAIDS) (2021): Feature story (2021); 2021. Figshare https://www.unaids.org/en/resources/presscentre/featurestories/2021/march/20210324tuberculosis-death speople-living-with-hiv. Accessed 2 June 2022.
42. Federal Democratic Republic of Ethipia Ministry of Health (FDREMoH). National Guidelines for TB, DR-TB and Leprosy in Ethiopia. Addis Ababa: Ministry of Health of Ethiopia; 2018.
43. Sánchez MS, Lloyd-Smith JO, Getz WM. Monitoring linked epidemics: the case of tuberculosis and HIV. PLoS One. 2010;5(1). https://doi.org/10.1371/journal.pone.0008796.
44. Aturinde A, Farnaghi M, Pilesjö P, Mansourian A. Spatial analysis of HIV-TB co-clustering in Uganda. BMC Infect Dis. 2019;19(1). https://doi.org/10.1186/s12879-019-4246-2.
45. Yirdaw KD, Jerene D, Gashu Z, et al. Beneficial effect of isoniazid preventive therapy and antiretroviral therapy on the incidence of tuberculosis in people living with HIV in Ethiopia. PLoS One. 2014;9(8). https://doi.org/10.1371/journal.pone.0104557.
46. Geremew D, Geremew H, Tamir M, Adem M, Tegene B, Bayleyegn B. Tuberculosis and isoniazid prophylaxis among adult HIV positive patients on art in northwest Ethiopia. PLoS One. 2022;17(4). https://doi.org/10.1371/journal.pone.0266803.
47. Nakiyingi L, Ssengooba W, Nakanjako D, et al. Predictors and outcomes of mycobacteremia among HIV-infected smear-negative presumptive tuberculosis patients in Uganda. BMC Infect Dis. 2015;15(1):1–8. https://doi.org/10.1186/s12879-015-0812-4.
48. Sabasaba A, Mwambi H, Somi G, Ramadhani A, Mahande MJ. Effect of isoniazid preventive therapy on tuberculosis incidence and associated risk factors among hiv infected adults in Tanzania: a retrospective

cohort study. BMC Infect Dis. 2015;19(1):1–8. https://doi.org/10.1186/s12879-019-3696-x.
49. Wei W, Wei-Sheng Z, Ahan A, Ci Y, Wei-Wen Z, Ming-Qin C. The characteristics of TB epidemic and TB/HIV co-infection epidemic: a 2007-2013 retrospective study in Urumqi, Xinjiang Province, China. PLoS One. 2016;14(10). https://doi.org/10.1371/journal.pone.0164947.
50. Pedroso AO, Gomes D, Sousa SML, et al. Temporal and spatial analysis techniques as potential tools for combating the HIV epidemic among young Brazilian Amazonian people: An ecological study. Trop Med Infect Dis. 2022;7(7). https://doi.org/10.3390/tropicalmed7070137.
51. Zaragoza BA, Hernández TM, Bustamante MLP, et al. Spatial and temporal distribution of tuberculosis in the state of Mexico. Mexico Sci World J. 2012. https://doi.org/10.1100/2012/570278.
52. Jiang L, Li Z, Huang J, et al. Spatiotemporal clusters of HIV/AIDS infections caused by drug use and heterosexual contact in Ruili city, China 1989–2016. BMC Infect Dis. 2019;19(1):1–9. https://doi.org/10.1186/s12879-019-4568-0.
53. Ross JM, Henry NJ, Dwyer-Lindgren LA, et al. Progress toward eliminating TB and HIV deaths in Brazil, 2001-2015: a spatial assessment. BMC Med. 2018;16(1):1–10. https://doi.org/10.1186/s12916-018-1131-6.
54. Gatrell A, Bailey T. Interactive spatial data analysis in medical geography. Soc Sci Med. 1996;42(6):843–55. https://doi.org/10.1016/0277-9536(95)00183-2.
55. Cuadros DF, Li J, Branscum AJ, et al. Mapping the spatial variability of HIV infection in Sub-Saharan Africa: Effective information for localized HIV prevention and control. Sci Rep. 2017;7(1). https://doi.org/10.1038/s41598-017-09464-y.

Publisher's Note